Supporting Information

$Ti_3C_2T_x$ MXene supported Ruthenium Nanoclusters for Efficient Electrocatalytic Hydrogen Evolution

Xuanyin Li [a], Dong Fang *[a], Jianhong Yi [a], Lang Zhang *[a], Jian Liu [b], Feng Liu [b]

[a]Advanced Power Materials Innovation Team, Faculty of Materials Science and Engineering, Kunming University of Science and Technology, Kunming, 650093, P. R. China. E-mail: fangdong@kmust.edu.cn; 3086818048@qq.com

[b]Yunnan Precious Metals Lab Co., Ltd., Kunming, Yunnan 650106, P. R. China.

Experimental Details

Synthesis of Ru@MXene-NS Catalyst: 50 mg of MXene-NS powder was dispersed in 50 ml of deionized water under continuous stirring to obtain an MXene-NS suspension. During stirring, 0.3 mmol of $RuCl_3$•xH_2O was added to the suspension and stirred until completely dissolved, followed by ultrasonication for 30 min in an ice bath. Subsequently, 10 ml of ethanol was added to the suspension and stirred for 10 min. The prepared suspension was then placed in a hydrothermal reactor and subjected to hydrothermal reaction at 180 ℃ for 2 h. The reaction mixture was transferred to a 50 ml centrifuge tube and washed several times with deionized water. Each wash was performed by centrifugation at 6000 rpm for 3 min. The resulting dispersion was freeze-dried for 48 h to collect the final product.

Synthesis of Ru@MXene-NF Catalyst: 50 mg of MXene-NF powder was dispersed in 50 ml of deionized water under continuous stirring to obtain an MXene-NF suspension. During stirring, 0.3 mmol of $RuCl_3$•xH_2O was added to the suspension and stirred until completely dissolved, followed by ultrasonication for 30 min in an ice bath. Subsequently, 10 ml of ethanol was added to the suspension and stirred for 10 min. The prepared suspension was then placed in a hydrothermal reactor and subjected to hydrothermal reaction at 120 ℃. Changing the time of the experiment in order to prepare Ru@MXene-NF (2 h) and Ru@MXene-NF (4 h) The reaction mixture was transferred to a 50 ml centrifuge tube and washed several times with deionized water. Each wash was performed by centrifugation at 6000 rpm for 3 min. The resulting dispersion was freeze-dried for 48 h to collect the final product.

Synthesis of Ru nanoparticle: 0.3 mmol of $RuCl_3$•xH_2O was dissolved in 50 ml of deionized water under continuous stirring. After complete dissolution, the solution was ultrasonicated for 30 min in an ice bath. Subsequently, 10 ml of ethanol was added and stirred for an additional 10 min. The prepared suspension was then placed in a hydrothermal reactor and subjected to hydrothermal reaction at 180 ℃ for 2 h. The reaction mixture was transferred to a 50 ml centrifuge tube and washed several times with deionized water. Each wash was performed by centrifugation at 6000 rpm for 3 min. The resulting dispersion was freeze-dried for 48 h to collect the Ru nanoparticles.

Synthesis of Ti_3C_2Tx MXene nanoparticle (MXene-NP): 50 mg of MXene-NF powder was dispersed in 50 ml of deionized water under continuous stirring to obtain an MXene-NF suspension. The prepared suspension was then placed in a hydrothermal reactor and subjected to hydrothermal reaction at 180 ℃ for 2 h. The reaction mixture was transferred to a 50 ml centrifuge tube and washed several times with deionized water. Each wash was performed by centrifugation at 6000 rpm for 3 min. The resulting dispersion was freeze-dried for 48 h to collect the MXene-NP.

Materials characterization

The microstructure was characterized with field emission scanning electron microscopy (SEM) of a Sigma 300 from ZEISS. Transmission electron microscopy (TEM), High-resolution transmission electron microscopy (HRTEM), selected area electron diffraction (SAED), and high-angle annular dark-field scanning transmission electron microscopy (HAADF-STEM) images obtained with a JEOL JEM-F200. XPS measurements were conducted using a Thermo Scientific K-Alpha X-ray photoelectron spectrometer. Inductively coupled plasma-mass spectrometry (ICP-MS) was conducted using an Agilent 5110. Brunauer-Emmett-Teller (BET) test was conducted using Micromeritics ASAP 2460.

Electrochemical Measurements

All the electrochemical measurements were carried out on an electrochemical workstation (CS350M, CORRTEST) in a standard three-electrode system at room temperature. The glassy carbon electrode (GCE, 3 mm in diameter) loaded with catalysts was used as the working electrode, while a mercurous sulfate electrode and an unused graphited rod were used as reference electrode and counter electrode, respectively, and 0.5 M H_2SO_4 (pH ≈ 0.3) was used as the electrolytes. The catalyst ink was prepared by mixing 5 mg of catalyst, 95 μL of ethanol, and 5 μl of Nafion solution (5 wt%) followed by ultrasonication until a homogeneous suspension was obtained. Then, 1.75 μl of the mixture was then carefully drop-cast onto the GCE.

For HER tests, linear sweep voltammetry (LSV) with iR-correction was carried out at a scan rate of 5 mV s^{-1}. Before LSV testing, cyclic voltammetry (CV) was performed at a scan rate of 100 mV s^{-1} for 10 cycles to stabilize the catalysts. Tafel slope was calculated based on LSV curves. The whole test data were converted to the reversible hydrogen electrode (RHE) according to the Nernst equation: E(RHE) = E(Hg/Hg_2SO_4) + 0.059 × pH + 0.656. Electrochemical impedance spectroscopy (EIS) tests were performed from 100 kHz to 0.1 Hz at the overpotential of 10 mA cm^{-2}. The double-layer capacitance (C_{dl}) was used to estimate the electrochemically active surface area (ECSA). CV was also performed in the scan rate from 20 to 100 mV s^{-1} for the double layer capacitance (C_{dl}) calculation. Cycling stability was assessed by CV conducted between 0.3 V and -0.1 V vs RHE at 100 mV s^{-1}. Chronopotentiometry measurements were recorded at a current density of 10 mA cm^{-2} for 40 h.

DFT calculations

The density functional theory (DFT) calculations were carried out with the VASP code.[1] The Perdew-Burke-Ernzerhof (PBE) functional within generalized gradient approximation (GGA)[2] was used to process the exchange–correlation, while the projector augmented-wave pseudopotential (PAW)[3] was applied with a kinetic energy cut-off of 500 eV, which was utilized to describe the expansion of the electronic eigenfunctions. The Brillouin-zone integration was sampled by a Γ-centered 7 × 7 × 1 Monkhorst-Pack k-point. All atomic positions were fully relaxed until energy and force reached a tolerance of 1 × 10^{-6} eV and 0.01 eV/Å, respectively. The dispersion corrected DFT-D method was employed to consider the long-range interactions.[4]

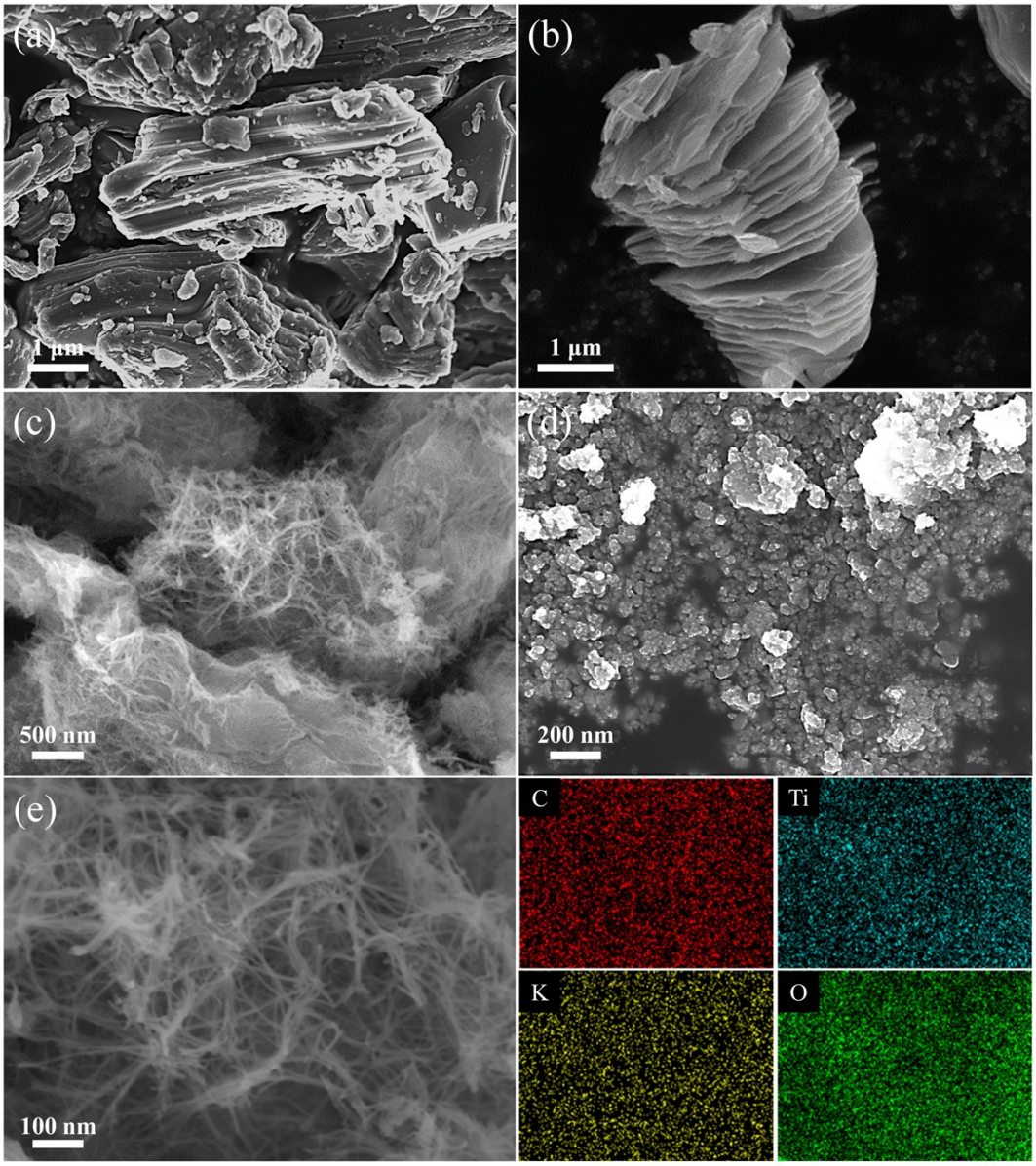

Fig. S1 SEM images of (a) MAX, (b) MXene-NS, (c) MXene-NF, and (d) Ru@MXene-NP; (e) SEM-EDS elemental mapping images of MXene-NF.

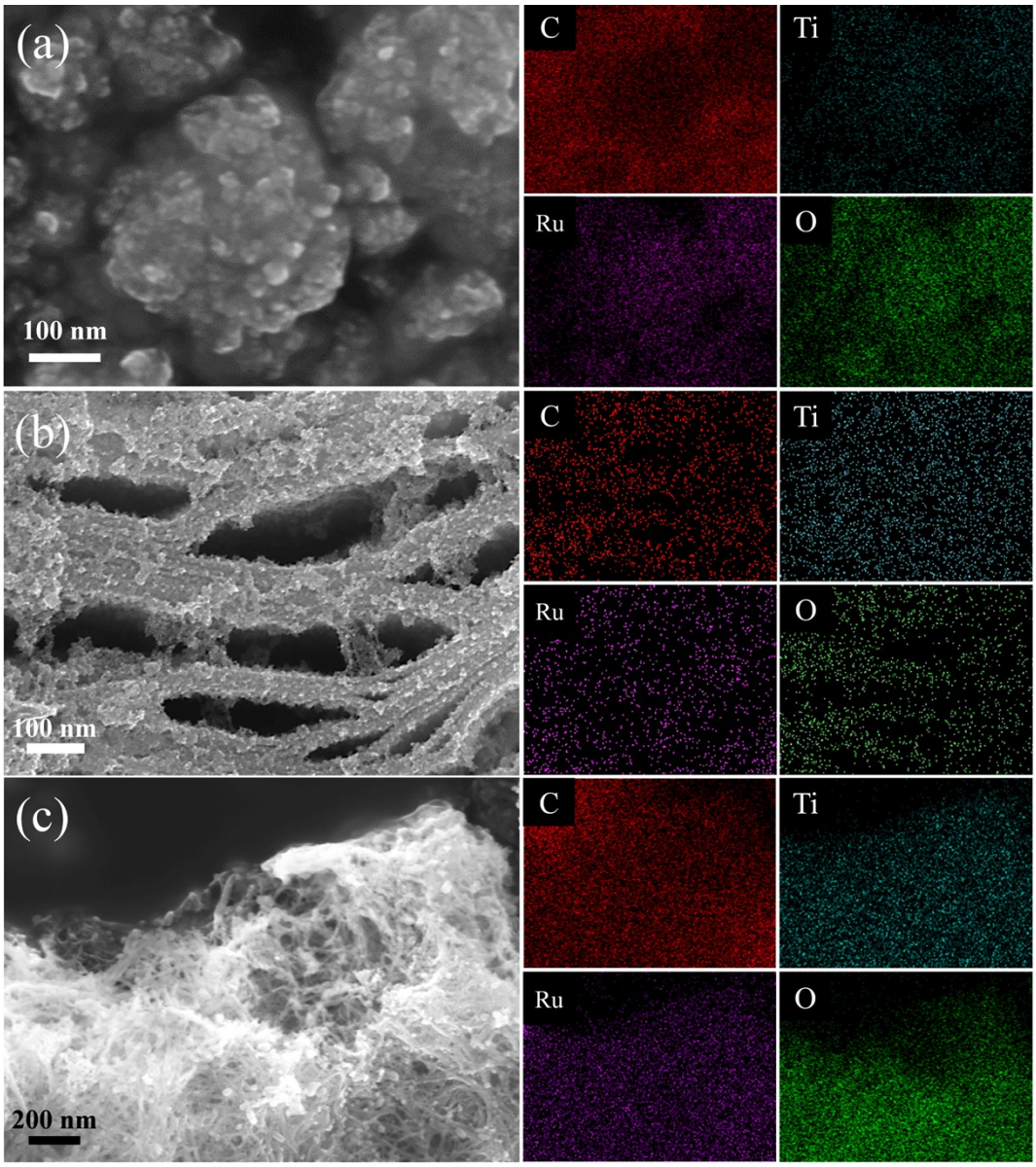

Fig. S2 SEM-EDS elemental mapping: (a) Ru@MXene-NP, (b) Ru@MXene-NS and (c) Ru@MXene-NF (2 h).

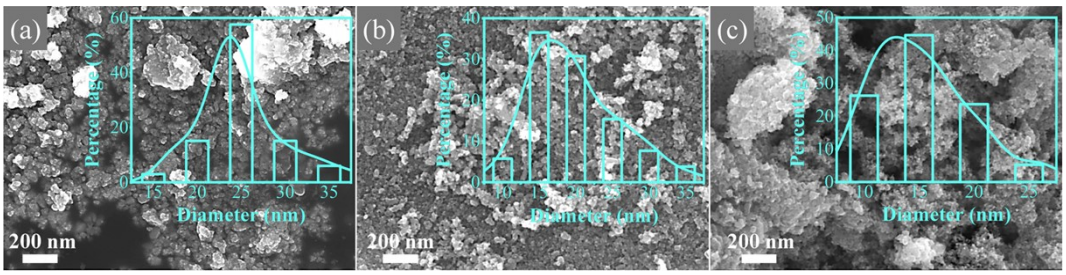

Fig. S3 Extended hydrothermal duration results in increased particle size. Hydrothermal conditions: 180 ℃, standard ruthenium sources and additions, alcohol: DI water = 1:5. Change the hydrothermal time: (a) 2 h, (b) 1 h and (c) 0.5 h.

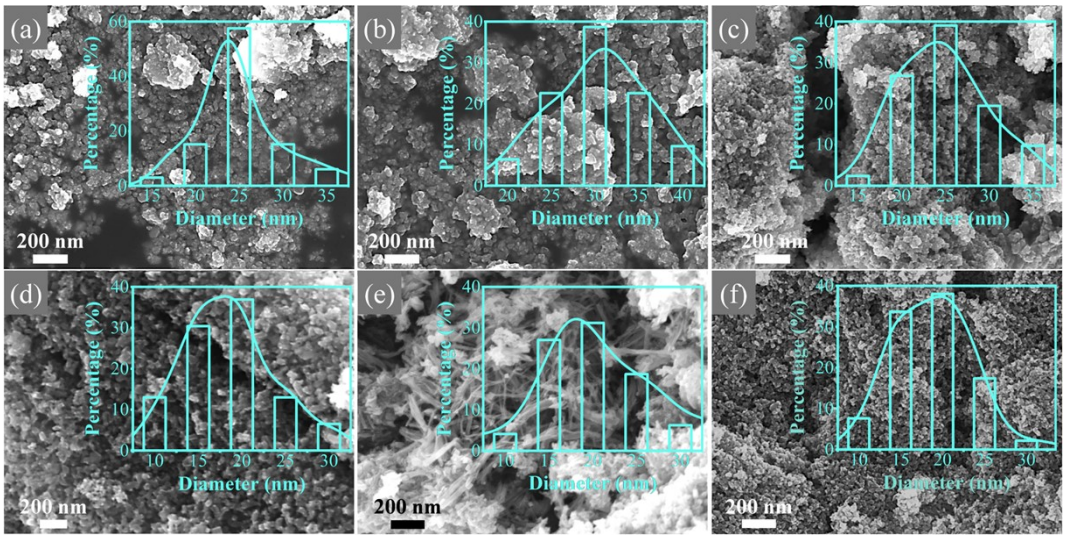

Fig. S4 The addition of alcohol during the hydrothermal process enhances material dispersion and inhibits particle growth. Hydrothermal conditions: 180 ℃, change the amount of added alcohol and hydrothermal conditions. (a) Standard ruthenium sources and additions, alcohol: DI water = 1:5, 2 h; (b) Standard ruthenium sources and additions, alcohol: DI water = 1:10, 2 h; (c) Standard ruthenium sources and additions, alcohol: DI water = 1:10, 1 h; (d) Standard ruthenium sources and additions, alcohol: DI water = 1:1, 2 h; (e) No ruthenium source added, alcohol: DI water = 1:5, 2 h; (f) No ruthenium source added, no alcohol, 2 h.

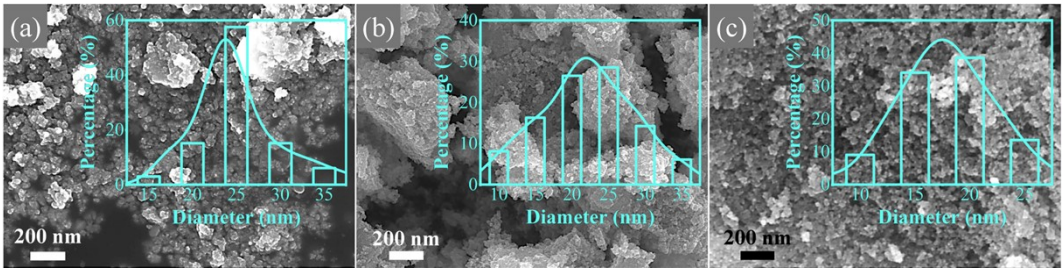

Fig. S5 Varying the amount of the added Ru source has a minimal effect on particle size. Hydrothermal conditions: 180 ℃, 2 h, alcohol: DI water = 1:5, change of ruthenium source conditions. (a) Standard ruthenium source ($RuCl_3$); (b) 1/12 of standard $RuCl_3$; (c) Standard ruthenium source ($Ru(acac)_3$).

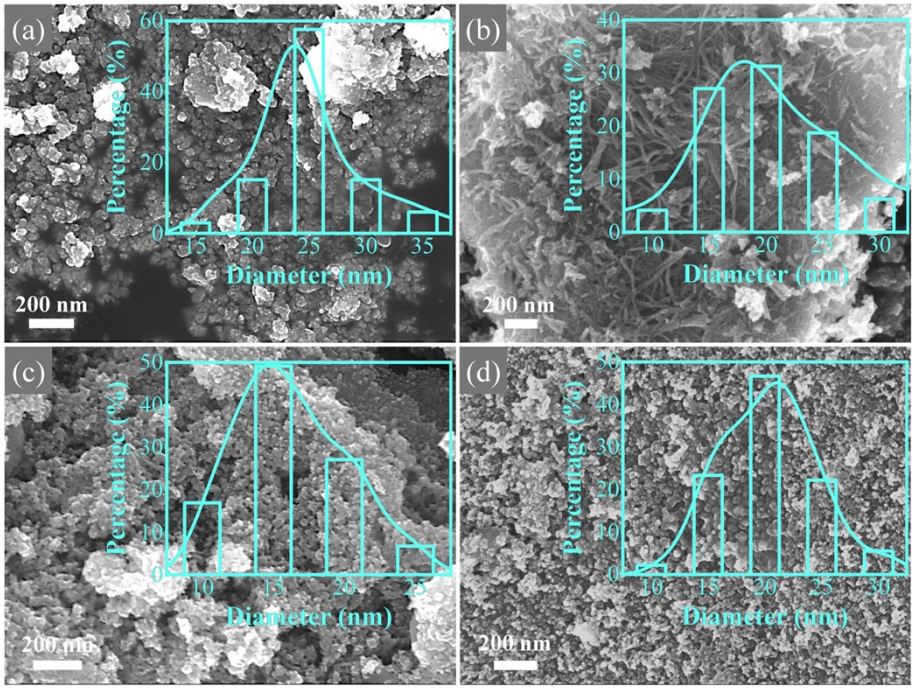

Fig. S6 Lower pH conditions promote the formation of larger nanoparticles. Hydrothermal conditions: 180 ℃, 2 h, alcohol: DI water = 1:5, change of pH and ruthenium source. (a) Standard ruthenium source ($RuCl_3$), PH≈1; (b) No addition of ruthenium source, PH ≈ 7; (c) Standard ruthenium source ($RuCl_3$), the addition of NaOH to change the PH to 7; (d) No addition of ruthenium source, the addition of HCl to change the PH to 1.

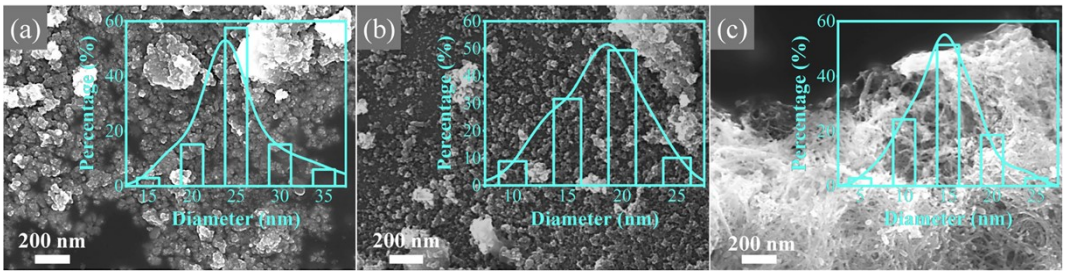

Fig. S7 Maintaining the low hydrothermal temperature helps retain the MXene-NF structure. Hydrothermal conditions: 2 h, standard ruthenium sources, and additions, alcohol: DI water = 1:5. Change the hydrothermal temperatures. (a) 180 ℃, (b) 150 ℃ and (c) 120 ℃.

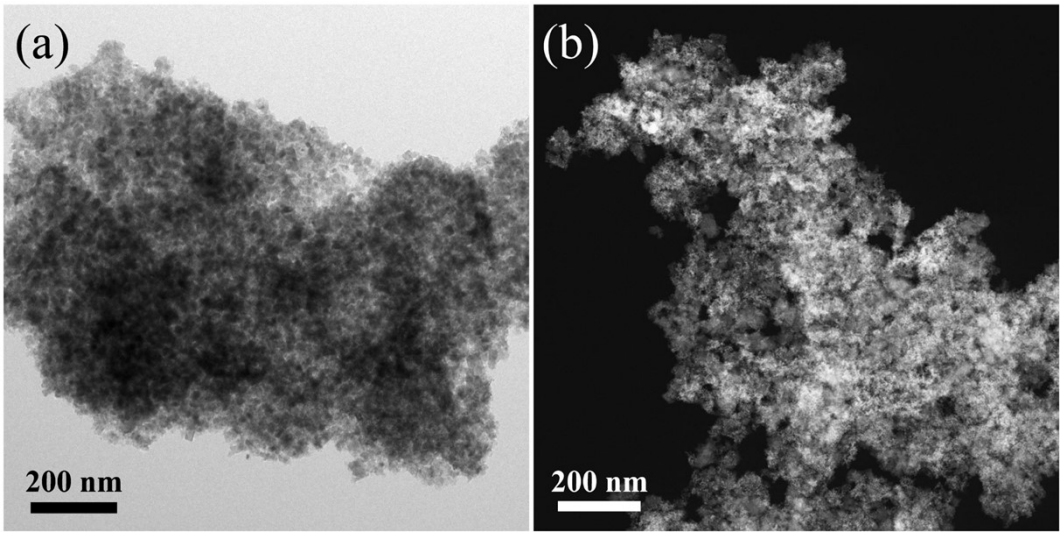

Fig. S8 (a) TEM image and (b) HAADF-STEM image of Ru@MXene-NP.

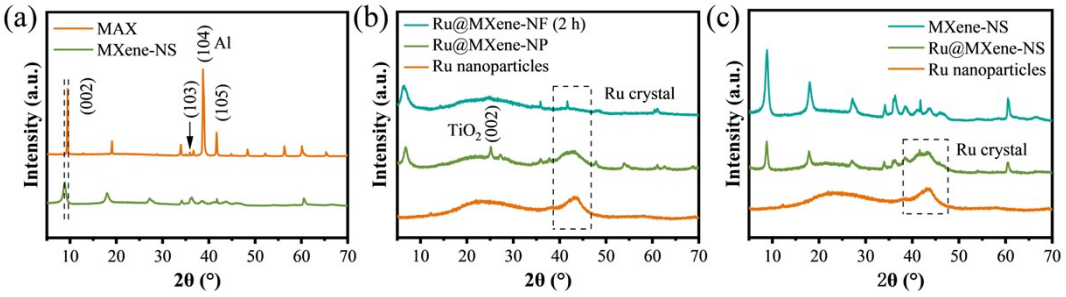

Fig. S9 XRD patterns: (a) MAX and MXene-NS; (b) Ru@MXene-NF (2 h), Ru@MXene-NP, and Ru nanoparticles; (c) MXene-NS, Ru@MXene-NS, and Ru nanoparticles.

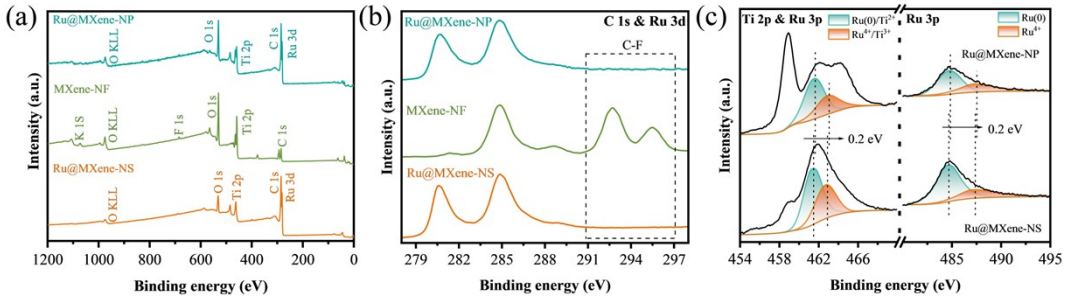

Fig. S10 (a) Full scan XPS spectra of Ru@MXene-NP, MXene-NF and Ru@MXene; XPS spectra of (b) C 1s & Ru 3d high-resolution XPS spectra for Ru@MXene-NP, MXene-NF and Ru@MXene-NS and (c) Ti 2p & Ru 3p and Ru 3p high-resolution XPS spectra for Ru@MXene-NP and Ru@MXene-NS.

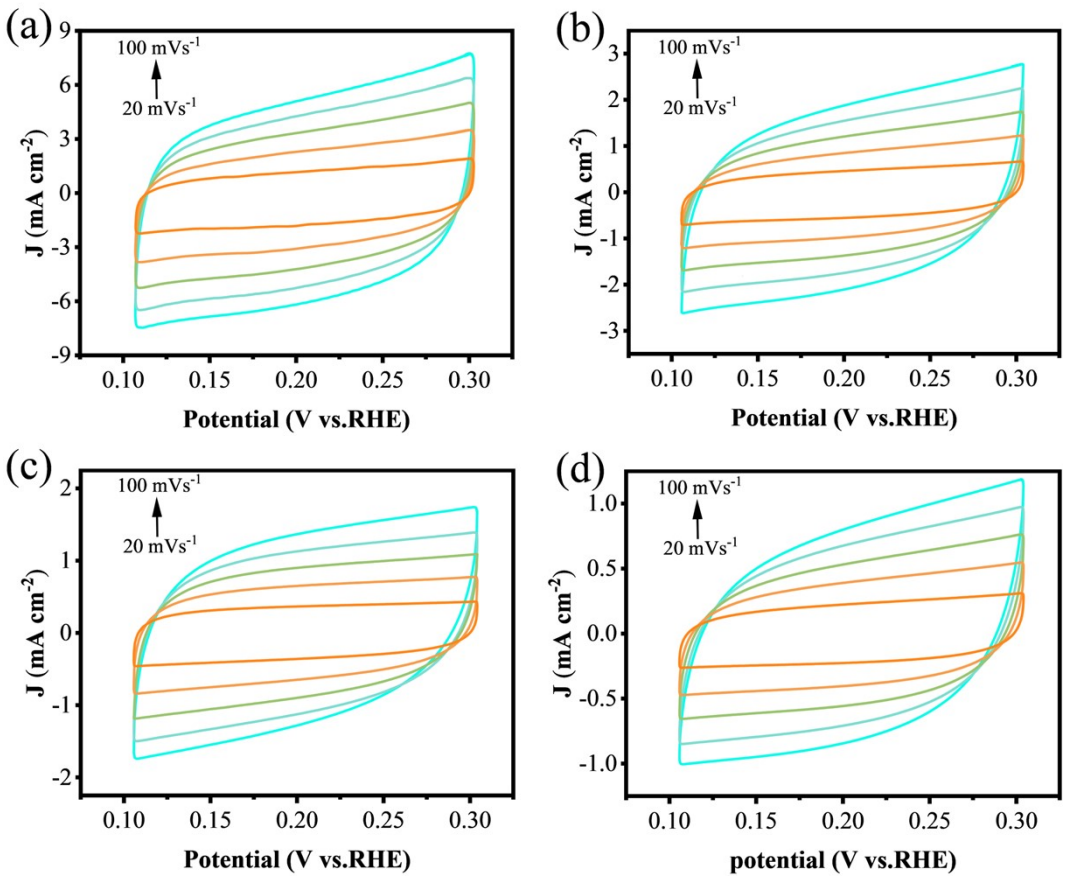

Fig. S11 CV curves at different scan rates in 0.5 M H_2SO_4 for HER of (a) Ru@MXene-NP, (b) Ru@MXene-NS, (c) MXene-NS, and (d) MXene-NF.

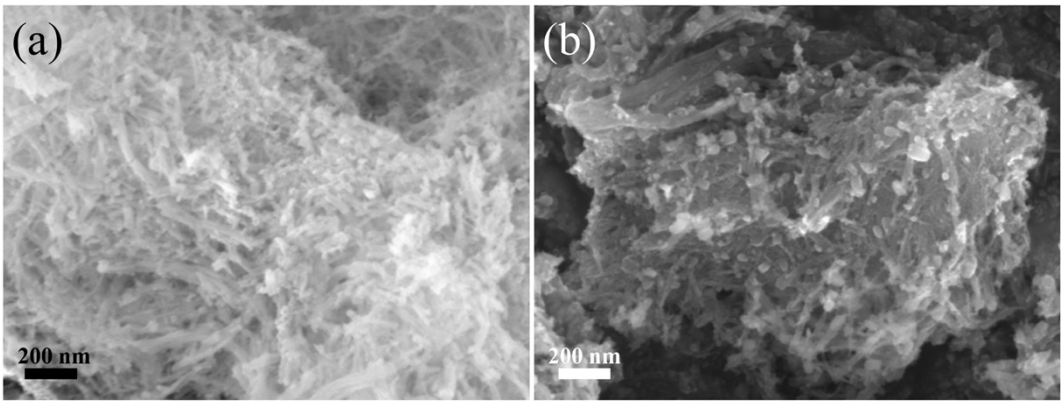

Fig. S12 TEM images of (a) Ru@MXene-NF (2 h) and (b) Ru@MXene-NF (4 h).

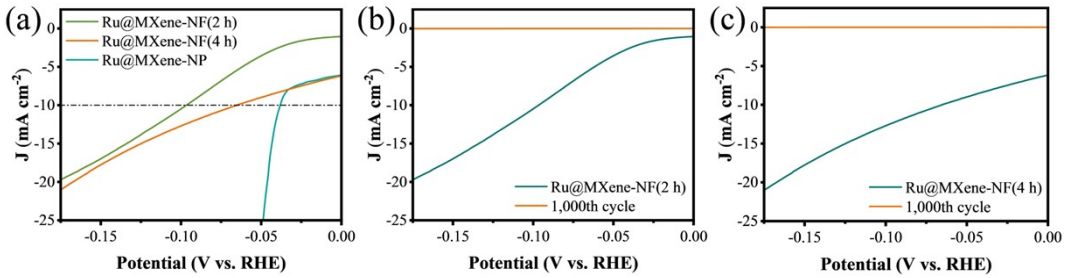

Fig. S13 (a) Polarization curves of Ru@MXene-NP, Ru@MXene-NF (2 h) and Ru@MXene-NF (4 h); (b) LSV curves of Ru@MXene-NF (2 h) at initial and after 1,000 CV cycles; (c) LSV curves of Ru@MXene-NF (4 h) at initial and after 1,000 CV cycles.

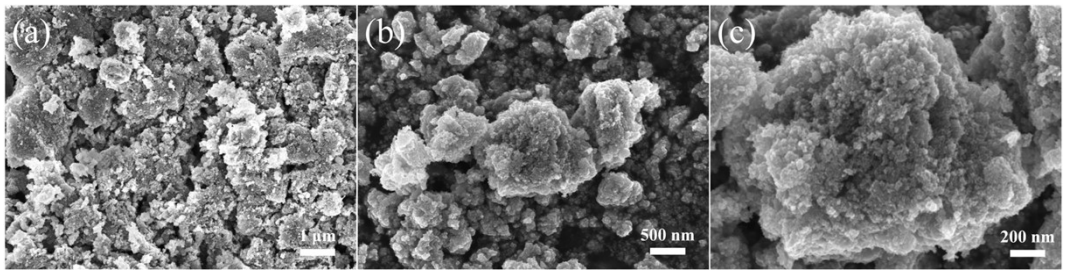

Fig. S14 SEM images of Ru@MXene-NP maintained stable HER activity over 10,000 CV cycles: (a) 1μm, (b) 500 nm and (c) 200 nm.

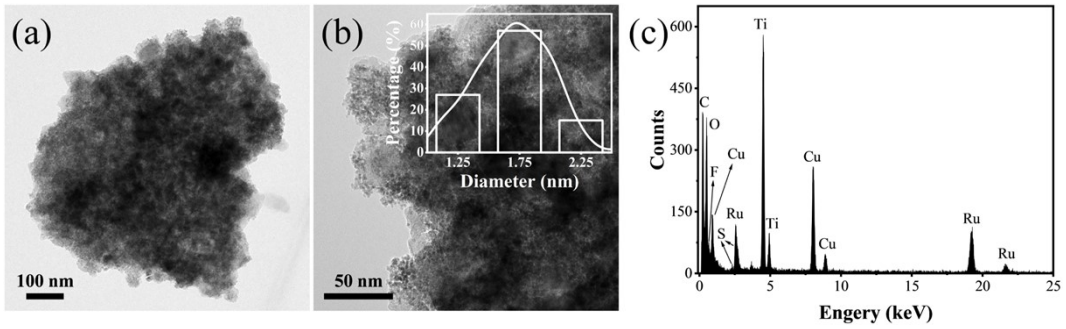

Fig. S15 (a, b) TEM images of Ru@MXene-NP maintained stable HER activity over 10,000 CV cycles; (c) The EDS composition of Ru@MXene-NP.

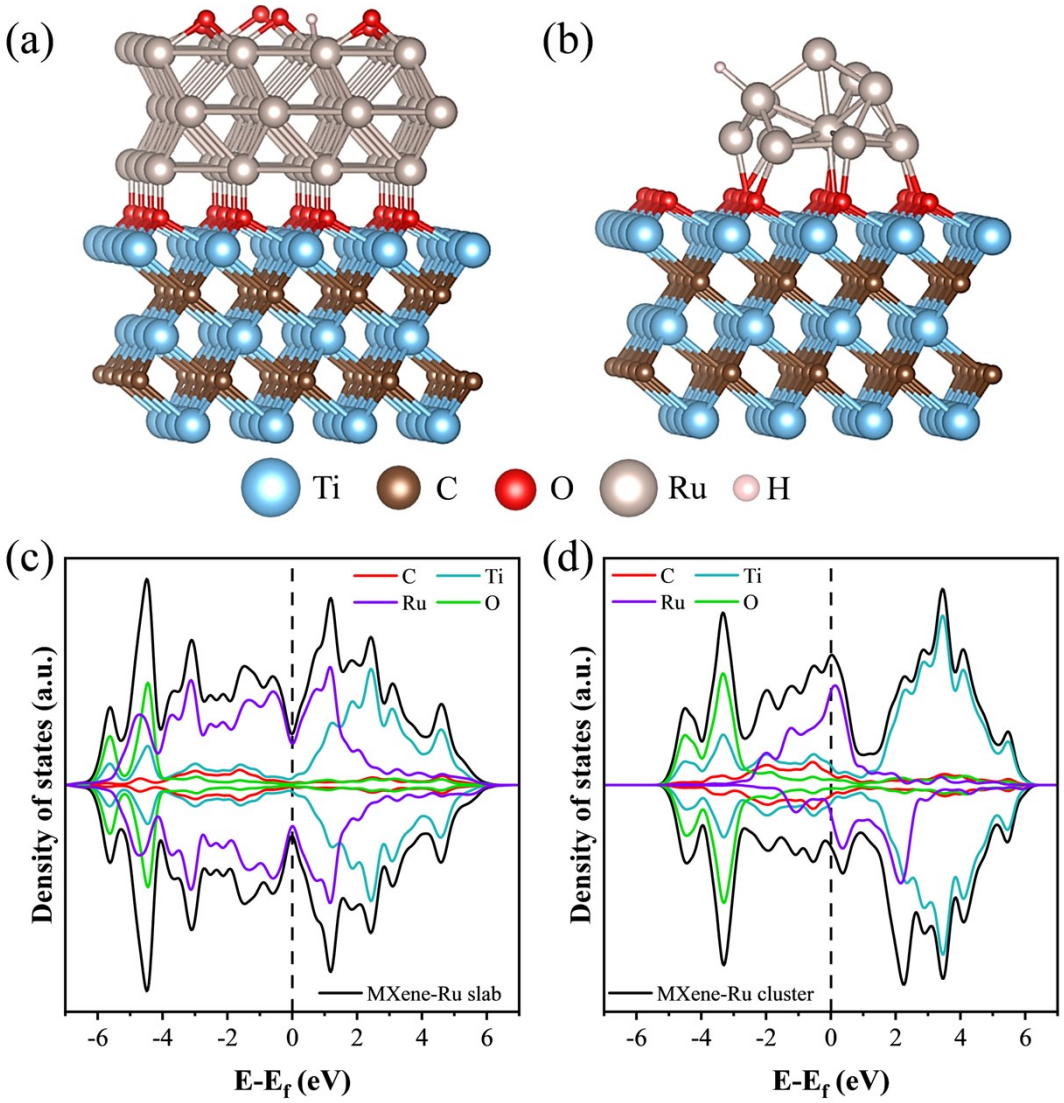

Fig. S16 The simulative models of (a) MXene-Ru slab and (b) MXene-Ru cluster; DOS curves: (c) MXene-Ru slab and (d) MXene-Ru cluster.

Table. S1 the Brunauer-Emmett-Teller (BET) of Ru@MXene-NP and Ru@MXene

Catalysts	BET Surface Area ($m^2 g^{-1}$)
Ru@MXene-NP	34.0352
Ru@MXene-NS	22.1584

Table. S2 Comparison of recent reported catalysts for HER in 0.5 M H_2SO_4.

Catalysts	Overpotential (mV) @10 mA cm^{-2}	Experimental conditions	Tafel slope (mV dec^{-1})	Refs.
Ru@MXene-NP	38.4	0.5M H_2SO_4	26.4	This work
Ru@MXene-NS	78.5	0.5M H_2SO_4	55.5	This work
RuSA@$MoSe_2$-MXene	49	0.5M H_2SO_4	50.9	5
Ru@1T-MoS_2-MXene	44	0.5M H_2SO_4	47	6
Ru@B-$Ti_3C_2T_x$	63	0.5M H_2SO_4	100	7
RuSA-N-S-$Ti_3C_2T_x$	76	0.5M H_2SO_4	90	8
RuSA/$Ti_3C_2T_x$	70	0.1M $HClO_4$	27.7	9
RuSA-N-$Ti_3C_2T_x$	23	0.5M H_2SO_4	42	10
Pt-V_2CT_x	27	0.5M H_2SO_4	30.8	11
Pt@N-$Ti_3C_2T_x$	11	0.5M H_2SO_4	35.2	12
Ru@V-RuO_2/C	46	0.5M H_2SO_4	55	13

Ru/Ru_{SA}-NMC	45	0.5M H_2SO_4	52	14
Ru-3/FNS	54	0.5M H_2SO_4	57	15
Ru@N-TiO_2/C	116	0.5M H_2SO_4	66	16
Ru@SC-CDs	59	0.5M H_2SO_4	52	17
NMC-Ru_{SA+NC}	16	0.5M H_2SO_4	66	18
Ru NCs/NC	32	0.5M H_2SO_4	33	19

1. G. Kresse and J. Furthmüller, *Comput. Mater. Sci*, 1996, **6**, 15-50.
2. J. P. Perdew, K. Burke and M. Ernzerhof, *Phys. Rev. Lett.*, 1996, **77**, 3865-3868.
3. P. E. Blöchl, *Physical Review B*, 1994, **50**, 17953-17979.
4. S. Grimme, *J. Comput. Chem.*, 2006, **27**, 1787-1799.
5. T. Ma, P. Wang, H.-J. Niu, Z. Che, G. Li and W. Zhou, *Carbon*, 2024, **218**, 118758.
6. G. Li, T. Sun, H.-J. Niu, Y. Yan, T. Liu, S. Jiang, Q. Yang, W. Zhou and L. Guo, *Adv. Funct. Mater.*, 2023, **33**, 2212514.
7. M. Bat-Erdene, M. Batmunkh, B. Sainbileg, M. Hayashi, A. S. R. Bati, J. Qin, H. Zhao, Y. L. Zhong and J. G. Shapter, *Small*, 2021, **17**, 2102218.
8. V. Ramalingam, P. Varadhan, H.-C. Fu, H. Kim, D. Zhang, S. Chen, L. Song, D. Ma, Y. Wang, H. N. Alshareef and J.-H. He, *Adv. Mater.*, 2019, **31**, 1903841.
9. X. Peng, S. Zhao, Y. Mi, L. Han, X. Liu, D. Qi, J. Sun, Y. Liu, H. Bao, L. Zhuo, H. L. Xin, J. Luo and X. Sun, *Small*, 2020, **16**, 2002888.
10. H. Liu, Z. Hu, Q. Liu, P. Sun, Y. Wang, S. Chou, Z. Hu and Z. Zhang, *J. Mater. Chem. A*, 2020, **8**, 24710-24717.
11. S. Park, Y.-L. Lee, Y. Yoon, S. Y. Park, S. Yim, W. Song, S. Myung, K.-S. Lee, H. Chang, S. S. Lee and K.-S. An, *"Appl. Catal., B"*, 2022, **304**, 120989.
12. Z. Kang, J. Cai, D. Ye, H. Zhao, J. Luo and J. Zhang, *Chem. Eng. J.*, 2022, **446**, 137443.
13. Y. Li, W. Wang, M. Cheng, Y. Feng, X. Han, Q. Qian, Y. Zhu and G. Zhang, *Adv. Mater.*, 2023, **35**, 2206351.
14. X. Wang, H. Yao, C. Zhang, C. Li, K. Tong, M. Gu, Z. Cao, M. Huang and H. Jiang, *Adv. Funct. Mater.*, 2023, **33**, 2301804.
15. C. Zhang, Y. Cui, C. Jiang, Y. Li, Z. Meng, C. Wang, Z. Du, S. Yu, H. Tian and W. Zheng, *Small*, 2023, **19**, 2301721.
16. W. Xu, H. Xie, F. Cao, S. Ran, Y. Duan, B. Li and L. Wang, *J. Mater. Chem. A*, 2022, **10**, 23751-23759.
17. Y. Liu, Y. Yang, Z. Peng, Z. Liu, Z. Chen, L. Shang, S. Lu and T. Zhang, *Nano Energy*, 2019, **65**, 104023.
18. H. Yao, X. Wang, K. Li, C. Li, C. Zhang, J. Zhou, Z. Cao, H. Wang, M. Gu, M. Huang and H. Jiang, *"Appl. Catal., B"*, 2022, **312**, 121378.
19. X. Huang, R. Lu, Y. Cen, D. Wang, S. Jin, W. Chen, I. Geoffrey, N. Waterhouse, Z. Wang, S. Tian and X. Sun, *Nano Res.*, 2023, **16**, 9073-9080.